BMC Medical Genomics

RESEARCH

Open Access

Whole-exome sequencing identifies *PRSS56* variants in Chinese patients with microphthalmia

Jingyi Luo[1,2], Kaijing Li[1], Runcai Yang[1], Mingjun Tang[1] and Jian Ge[1*]

Abstract

Purpose This study aimed to elucidate the genetic and clinical profiles of Chinese patients with microphthalmia harbouring *PRSS56* variants and investigate the genotype–phenotype correlation.

Methods Whole-exome sequencing (WES) was performed in patients with microphthalmia and available family members to assess coding regions and adjacent intronic splice boundaries for variant detection and downstream interpretation. The axial lengths (ALs) of all the probands and available family members were measured. The genotype–phenotype correlation was explored by statistical analysis, and protein structure prediction was analysed in silico.

Results Seven *PRSS56* variants were detected across four of the seven families, including two novel candidate variants (c.175G > A:p.E59K and c.1030 C > A:p.P344T) and five previously reported variants. Variant p.Q356Pfs152 was found in two unrelated families and was the most frequent. The mutational spectrum frequency in the Chinese population differed from that in other ethnic groups worldwide. The average AL was 17.82 ± 1.51 mm. In an exploratory pooled analysis combining the current cohort with previously published cases, eyes with biallelic LoF variants showed shorter ALs than eyes with missense variants. Variants p.G107V and p.E396K, which were reported exclusively in Chinese microphthalmia cases, were predicted to destabilize the PRSS56 protein.

Conclusions Among nine individuals from seven families, seven *PRSS56* variants were identified in four families, underscoring the significant genetic diversity within the Chinese population. The reported variant p.Q356Pfs*152 had the highest frequency in our cohort. Our findings expand current understanding of *PRSS56*-associated microphthalmia and provide valuable information for prenatal diagnosis and future therapeutic strategies.

Keywords Microphthalmia, *PRSS56*, Whole-exome sequencing, Genotype–phenotype correlation

*Correspondence:
Jian Ge
gejian@mail.sysu.edu.cn
[1]State Key Laboratory of Ophthalmology, Guangdong Provincial Key Laboratory of Ophthalmology and Visual Science, Zhongshan Ophthalmic Center, Sun Yat-sen University, Guangzhou, Guangdong 510060, China
[2]Department of Ophthalmology, The Third Affiliated Hospital, Sun Yat-sen University, Guangzhou, Guangdong 510630, China

Background

Microphthalmia, including two major subtypes nanophthalmos and posterior microphthalmia, is an ocular abnormality presents as symmetrically or asymmetrically reduced axial length (AL), high hyperopia, and occasional angle-closure glaucoma (ACG) [1, 2]. Microphthalmia significantly affects vision function, as complications, including cataracts, ACG, uveal effusion, retinal degeneration, strabismus, and more [3–7], substantially impair the quality of patients' life. The molecular pathogenesis of microphthalmia remains elusive, and genetic regulation is considered to contribute to the maldevelopment of the eyeball. We previously reported 14 trios and 10 sporadic cases of microphthalmia and identified three de novo variants in *MYRF*, as well as inherited variants in *MYRF*, *MFRP*, and *PRSS56*[2]. Nevertheless, in a subsequent study with newly enrolled patients with microphthalmia, we identified 16 variants of *MFRP* in 17 Chinese families, further expanding the genetic knowledge of microphthalmia [8].

The *PRSS56* (MIM: 613858) gene encodes a 603-amino acid protein called protease serine 56, which has an N-terminal signal peptide, a chymotrypsin-like serine protease domain, and a C-terminal conserved domain. In the human eye, PRSS56 is expressed predominantly in the neural retina and optic nerve and is also present in the cornea, uvea, sclera, and trabecular meshwork [9]. PRSS56 plays an important role in determining ocular size, and the *PRSS56* variants have been implicated in both hyperopia and myopia progression [10, 11]. It has been demonstrated that loss-of-function (LoF) variants in *PRSS56* result in reduced ocular size, hyperopic refractive error, ACG, and abnormal ocular drainage structures in genetic mouse models [12–14]. Similar phenotypes were also observed in humans, as patients with biallelic *PRSS56* variants typically present with posterior microphthalmos or nanophthalmos, characterized by markedly short axial length, severe hyperopia, a high frequency of ACG, and retinopathy, such as horizontal papillomacular retinal folds, foveal hypoplasia, and uveal effusion [12,15,16]. In the Chinese population, mutation analyses of *PRSS56* in microphthalmia have been limited [2, 10]. Recently, Li et al. reported the clinical features of patients with nanophthalmos harbouring mutations in four genes, including *PRSS56*, whereas the individual parameters were not detailed [17].

Considering this, we aimed to characterize the *PRSS56* variants and clinical characteristics in patients with microphthalmia from seven unrelated Chinese families to better understand this rare disease and expand the mutation spectrum of *PRSS56* within the Chinese population.

Methods

Study participants and clinical examinations

This was a retrospective clinical case series. A cohort of nine individuals diagnosed with microphthalmia, representing seven unrelated families, was enrolled at Zhongshan Ophthalmic Center (ZOC), Sun Yat-sen University (Guangzhou, China), between January 2023 and December 2023. Written informed consent was obtained from all participants or their legal guardians. The study followed the principles outlined in the Declaration of Helsinki and was approved by the Human Research Ethics Committee of ZOC.

The inclusion criteria were (1) a clinical diagnosis of microphthalmia supported by ocular biometry: AL < 20 mm in adults, which may or may not be accompanied by structural ocular abnormalities [8], and the terms "posterior microphthalmia" and "nanophthalmos" grouped together under the general term "microphthalmia", reflecting the hypothesis that they may share underlying genetic causes; (2) a phenotype with extreme refractive error and imaging features judged by the treating ophthalmologists to be consistent with a developmental microphthalmia disorder; and (3) the availability of DNA of sufficient quality for next-generation sequencing analysis. The exclusion criteria were (1) evidence of secondary or acquired causes that could explain a reduced AL or a small-eye appearance, such as prior ocular trauma and severe intraocular inflammation; (2) a confirmed alternative genetic diagnosis explaining the phenotype before or during analysis; and (3) inadequate clinical information to support case definition and DNA not meeting quality requirements for sequencing.

As we previously described [8], all participants underwent a comprehensive ophthalmic assessment. Evaluations included measurements of best-corrected visual acuity (BCVA) and intraocular pressure (IOP) using Goldmann applanation tonometry, slit-lamp biomicroscopy with gonioscopy, and fundus examination. Axial length was determined using A-scan ultrasonography. Ultrasound biomicroscopy (Model SW-3200 L, Suoer Electronic Ltd., Tianjin, China), colour fundus photography (Kowa, Tokyo, Japan), optical coherence tomography, ocular biometry (IOLMaster 700; Carl Zeiss Meditec AG), and B-scans (Cinescan A/B scan, Quantel Medical, Clemon, France) were performed when available.

Whole-exome sequencing (WES) and variant analysis

Blood samples were obtained from all participants who were available for collection. Genomic DNA was isolated using the QIAamp DNA Blood Mini Kit (Qiagen, Hilden, Germany). WES and variant analysis were performed as previously described [8, 18]. Briefly, purified genomic DNA was randomly fragmented and purified using magnetic beads. Fragmented DNA was end-repaired,

A-tailed, ligated to sequencing adapters, and PCR-amplified to generate pre-capture libraries. Libraries were captured using the xGen Exome Research Panel (Integrated DNA Technologies, Skokie, IL, USA) to enrich exonic regions, followed by post-capture enrichment and purification. The enriched libraries were sequenced on the NovaSeq 6000 platform (Illumina, San Diego, CA, USA) according to the manufacturer's instructions. The mean depth of coverage exceeded 300×, and > 99.5% of target regions were covered. Raw reads in FASTQ format were quality-filtered to generate clean reads and then aligned to the human reference genome (UCSC hg38) using the Burrows-Wheeler Aligner (BWA) [19]. Resulting BAM files were processed with Picard and the Genome Analysis Toolkit (GATK, Version 4.6.1) [20] for duplicate marking and base quality score recalibration. Single-nucleotide variants (SNVs) and small insertions/deletions (indels) were called using GATK HaplotypeCaller, followed by standard variant-level quality filtering. Variants within the *PRSS56* coding regions and the adjacent ± 30 bp exon–intron boundaries (RefSeq transcript NM_001195129.1) were extracted for downstream evaluation.

All variants were annotated according to the Human Genome Variation Society (HGVS; https://www.hgvs.org/mutnomen/) nomenclature and cross-referenced with the Human Gene Mutation Database (HGMD; https://www.hgmd.cf.ac.uk/ac/validate.php) to assess prior reports. Variants were not prioritized in the primary screen if they met any of the following criteria: low sequencing quality (coverage depth < 5×) or minor allele frequency > 0.01 in population databases (including 1000 Genomes Project [1000G] and the Genome Aggregation Database [gnomAD]). Synonymous, untranslated region, and non-canonical splice-region variants were assessed in a secondary review, but no additional compelling candidate variants were identified. The remaining variants were classified as pathogenic, likely pathogenic, or variants of uncertain significance (VUS) according to the American College of Medical Genetics and Genomics (ACMG) guidelines [21]. ClinVar (https://www.ncbi.nlm.nih.gov/clinvar/?term=PRSS56%5Bgene%5D) and LOVD (https://databases.lovd.nl/shared/variants/PRSS56) classifications were also provided for reference. For variants with conflicting in silico predictions, final classification was based on integrated ACMG evidence rather than on the number of tools supporting pathogenicity. Only variants that passed the applied quality filters were retained for annotation and interpretation. Exon numbering in schematic figures followed Ensembl transcript PRSS56-202 (ENST00000617714.2). The allele frequency of specific high-frequency variants were queried in NyuWa (Chinese Genome Database; http://bigdata.ibp.ac.cn/NyuWa_variants/index.php) and Westlake Bio-Bank for Chinese (WBBC; https://wbbc.westlake.edu.cn/index.html). All candidate variants were validated via Sanger sequencing; primer sequences and Sanger sequencing results were provided in the Supplementary Material (Table S1-S2).

Protein structure prediction

The amino acid sequence of human *PRSS56* (UniProt ID: P0CW18; 603 amino acids; isoform NP_001182058) was retrieved from the UniProt database (UniProt, 2024). As no experimentally resolved structure of PRSS56 is currently available, three-dimensional models of both wild-type and mutant proteins were generated using AlphaFold 3 [22]. Mutated protein sequences were derived from their corresponding DNA-level variants. Structural analyses, including visualization of protein conformation and hydrogen bonding for the p.G107V and p.E396K variants, were performed using PyMOL (PyMOL Molecular Graphics System, version 3.0; Schrödinger, LLC) and LigPlot + [23]. To evaluate the thermodynamic impact of nonsynonymous single nucleotide polymorphisms (nsSNPs), the change in Gibbs free energy (ΔΔG, kcal/mol) was computed using DUET, SDM, and mCSM—tools widely applied for predicting protein stability alterations induced by point mutations [24–26].

Statistical analyses

For the genotype–phenotype analysis, we included published data from recently published *PRSS56*-related Chinese microphthalmia cases for analysis [27]. Only cases with extractable individual-level AL (< 20 mm) data together with corresponding *PRSS56* variants were included; cases lacking patient-level AL data or with potentially overlapping cases were excluded. All statistical analyses were performed using GraphPad Prism (version 9.0; GraphPad, Inc., USA). Data normality was assessed using the Kolmogorov–Smirnov test. For comparisons between two groups, independent samples *t*-test was used if the data were normally distributed; otherwise, the Mann−Whitney *U* test was applied. For comparisons among three groups, the Kruskal−Wallis test was used for nonnormal data, which was followed by post hoc pairwise comparisons using Dunn's test with Bonferroni adjustment. A p value < 0.05 was considered to indicate statistical significance.

Results

Novel and known variants in *PRSS56*

Seven unrelated families with microphthalmia were recruited from four provinces in China, including three from Guangdong Province, two from Hainan Province, one from Guangxi Province, and one from Hubei Province. Among these seven unrelated Chinese families with

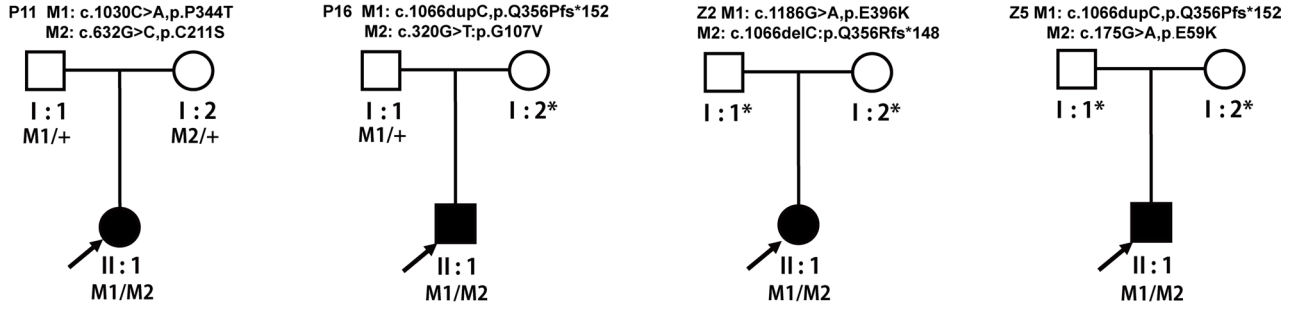

Fig. 1 Pedigrees of four Chinese families with microphthalmia linked to *PRSS56* variants. Asterisks * indicate family members who have not undergone clinical or genetic assessment

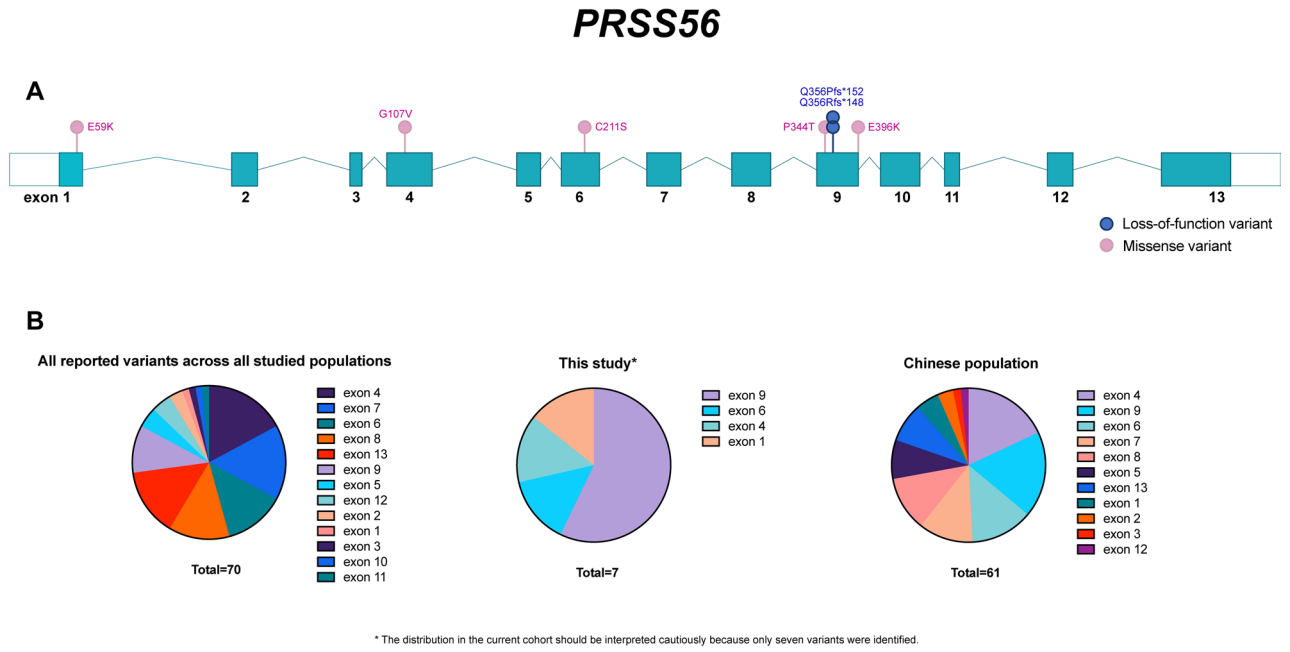

Fig. 2 Schematic representation of the *PRSS56* gene and its variants. **A** Schematic structure of the *PRSS56* gene showing the locations of all the variants identified in this study. N, amino terminus; C, carboxyl terminus. Exon numbering is based on Ensembl transcript PRSS56-202 (ENST00000617714.2; GRCh38). **B** The exonic-specific distribution of *PRSS56* variants identified in the literature, in the current study, and in the Chinese population (including previously and currently reported variants). The studied populations included Chinese, Caucasian/European, Turkish, Kurdish, Japanese, Arab, and South Asian ethnic groups.

microphthalmia, seven variants in *PRSS56* were identified in four families, whereas no pathogenic or likely pathogenic variants in *PRSS56* or other established microphthalmia-related genes were identified in the remaining three families by our WES analysis (Fig. 1). Two probands (from Families P11 and P16) carried compound heterozygous variants, and two probands (from Families Z2 and Z5) carried two variants for which phase could not be confirmed because parental testing was unavailable (Fig. 2A). Two novel candidate variants (c.175G > A:p.E59K and c.1030 C > A:p.P344T) and five reported variants (c.320G > T:p.G107V, c.632G > C:p.C211S, c.1066dupC: p.Q356Pfs*152, c.1066delC: p.Q356Rfs*148, c.1186G > A:p.E396K) were detected in *PRSS56* (Table 1, Supplementary Material Table S3). Two variants were classified as pathogenic, three were classified as likely pathogenic, and two variants were catalogued as VUS under ACMG criteria. There were five missense variants and two frameshift variants. Loss-of-function (LoF) variants of *PRSS56* were detected in three patients. No split reads or read depth comparable to that of the remaining portions of *PRSS56* were detected, suggesting that no exon-level CNVs were detected. The variants found in our study were predominantly located in Exon 9 (4/7, 57.14%) (Fig. 2B). A known variant, p.Q356Pfs*152, was found in two probands (50%), with allele frequencies of 2.23214e-4 in the WBBC database and 3.3344e-4 in the NyuWa database in the Chinese population. Two variants previously reported only in Chinese microphthalmia,

Table 1 *PRSS56* variants detected in our study

Exon	Nucleotide and amino acid change	Mutation Type	Bioinformatic analysis*			Allele Frequency in gnomAD	ACMG classification	ACMG Evidence	HGMD	ClinVar	LOVD	First Report
			CADD	SIFT	Polyphen-2							
1	c.175G > A:p.E59K	Missense	24.4	D	B	//	VUS	pm2 pp4	//	Uncertain significance	//	This study
4	c.320G > T:p.G107V	Missense	28.5	D	PrD	//	Likely pathogenic	pm1 pm2 pm5 pp4	DM	Likely pathogenic	VUS	Li et al.
6	c.632G > C:p.C211S	Missense	28.8	D	PrD	0.0000637877	Likely pathogenic	pm1 pm2 pp1 pp4	//	Likely pathogenic	VUS	Wen et al.
9	c.1030 C > A:p.P344T	Missense	27.6	D	PrD	//	VUS	pm2 pp1 pp3 pp4	//	Uncertain significance	//	This study
9	c.1066dupC:p.Q356Pfs*152	Frameshift insertion	22.6	//	//	0.000323855	Pathogenic	pvs1 pm2 pp1 pp4	DM	Pathogenic/Likely pathogenic	Pathogenic/Likely pathogenic	Gal.et al.
9	c.1066delC:p.Q356Rfs*148	Frameshift deletion	11.18	//	//	0.000064771	Pathogenic	pvs1 pm2 pp1 pp4	DM	Pathogenic	Pathogenic	Prasov et al.
9	c.1186G > A:p.E396K	Missense	27	D	B	//	Likely pathogenic	pm1 pm2 pp1 pp4 pp5	DM	Likely pathogenic	Likely pathogenic/VUS	Guo et al.

ACMG The American College of Medical Genetics and Genomics guidelines, *CADD* Combined Annotation-Dependent Depletion (https://cadd.gs.washington.edu/), SIFT (https://sift.bii.a-star.edu.sg/), Polyphen-2 (http://genetics.bwh.harvard.edu/pph2/), ClinVar (https://www.ncbi.nlm.nih.gov/clinvar/), LOVD (https://databases.lovd.nl/) *gnomAD* Genome Aggregation Database (https://gnomad.broadinstitute.org/), *DM* Disease-causing mutations, // = absent or no available, *VUS* variant of unknown significance

*None of the variants were present in the REVEL, PROVEAN, or HSF databases

Table 2 Clinical characteristics of patients with *PRSS56*-related microphthalmia in our cohort

Family	Age/	BCVA	AL (mm)	Refraction (D)	AC	Variant (cDNA, protein)					
Patient	Gender	OD	OS	OD	OS	OD	OS	OD	OS	Allele 1	Allele 2
Z2,II:1	47/F	20/100	20/70	16.89	16.66	+11.00	+12.00	no	no	c.1186G > A:p.E396K	c.1066delC: p.Q356Rfs*148
P11,II:1	32/F	20/100	20/100	18.91	19.02	NA	NA	no	no	c.1030 C > A,p.P344T	c.632G > C:p.C211S
P16,II:1	39/M	20/50	20/40	16.13	16.05	+9.50	+10.00	AC	AC	c.1066dupC, p.Q356Pfs*152	c.320G > T:p.G107V
Z5,II:1	41/M	20/50	20/100	19.28	19.58	+5.25	+5.00	no	no	c.1066dupC, p.Q356Pfs*152	c.175G > A,p.E59K

BCVA Best corrected visual acuity, *AL* Axial length, *AC* Angle closure

p.G107V and p.E396K, were found in one proband in our study.

Clinical findings and genotype–phenotype correlations

The clinical findings of the four patients with *PRSS56*-associated microphthalmia, including two males and two females, with an average age of 39.75 ± 6.18 years, are summarized in Table 2. All patients had ALs < 20 mm in both eyes. The average AL was 17.82 ± 1.51 mm (ranging from 16.13 to 19.58 mm). The clinical examinations of a representative patient with microphthalmia are presented in Fig. 3.

As Nowilaty et al. [28] previously reported that biallelic truncating *PRSS56* variants were associated with shorter ALs than biallelic missense *PRSS56* variants or no identified variant, we next investigated the correlations in ALs among different mutation types. Although all the microphthalmia eyes in our study had ALs longer than 16 mm, *PRSS56*-related microphthalmia eyes with LoF variants demonstrated a higher likelihood of having an AL less than 16 mm in previous studies (42/56, 75%) (from 37 studies regarding *PRSS56*-associated microphthalmia with specific individual AL data in PubMed until July 2025).

After compiling the ALs of 24 eyes from 12 patients reported in the previous study, we performed an exploratory pooled analysis comparing the ALs among eyes with biallelic LoF variants, monoallelic LoF variants, and biallelic or monoallelic missense variants. The results revealed that ALs in eyes with biallelic LoF variants were significantly shorter than those in eyes with missense variants (Fig. 4A). Additionally, no significant difference in ALs was observed when *PRSS56* variants (16.05 ± 1.23 mm) were compared with *MFRP* variants (16.02 ± 1.05 mm) in our cohort [8] ($p = 0.66$; Fig. 4B).

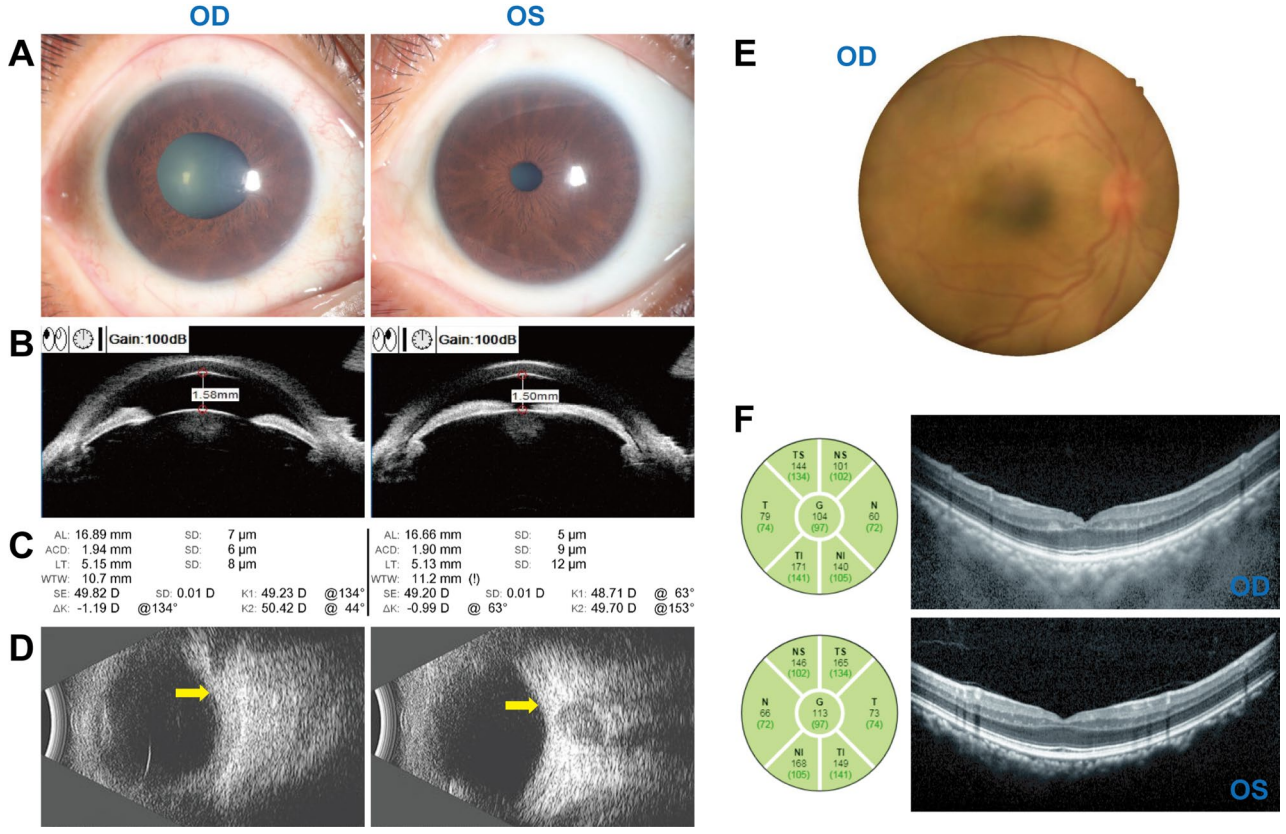

Fig. 3 Clinical examinations of representative patients with *PRSS56*-associated microphthalmia. A 47-year-old female presented with complaints of redness, pain, and impaired vision in the right eye. Her best-corrected visual acuities were counting fingers (right) and 0.2 (left), and her IOPs were 56 mmHg (right) and 15 mmHg (left). The refractions were +11 D (right) and +12.0 D (left). **A** Clinical examinations of the anterior segment revealed a shallow anterior chamber depth (ACD) in both eyes, with corneal oedema and moderate pupil dilation in the right eye. **B** Ultrasound biomicroscopy showed iris deformation; the ACDs were 1.58 mm (right) and 1.50 mm (left), and the peripheral anterior chamber angles were closed in the right eye and narrow but open in the left eye. **C** IOLMaster examination revealed axial lengths of 16.89 mm (right) and 16.66 mm (left), corneal powers of 49.82 D (right) and 49.20 D (left), and white-to-white corneal diameters of 10.7 mm (right) and 11.2 mm (left). **D** B-scan ultrasound revealed increased sclerochoroidal thickness (arrows) of 1.5 mm (right) and 1.6 mm (left) (yellow arrows). **E** Fundus image demonstrating a crowded disc, vascular dilation and tortuosity in the right eye. A qualified image was unavailable from the left eye because of the small pupil size and poor cooperation. **F** OCT showed mild foveal hypoplasia, punctate hyperreflective foci in the ganglion cell layer and inner nuclear layer, and a normal thickness of the retinal nerve fiber layer. The patient was diagnosed with acute primary angle closure, microphthalmia, and high hyperopia. After bilateral laser peripheral iridotomy, the IOPs were normal in both eyes

Protein structure prediction

As the p.G107V and p.E396K variants were detected in more than one proband and their protein structure had never been predicted, we subsequently used the bioinformatic analysis software AlphaFold3, PyMOL, and LigPlot + to predict their protein structures (Fig. 5A). Both the p.G107V and p.E396K variants were predicted to alter hydrogen bonds at the target amino acids. With respect to p.G107V, PyMOL and LigPlot+ predicted that the WT structure has hydrogen bonds between Gly107 and surrounding amino acids, while these bonds are lost after mutation (Fig. 5B–C), indicating its alteration of biological function. With respect to p.E396K, PyMOL showed that Glu396 was located in the middle of the α-helix structure and formed hydrogen bonds with Arg392, Arg393, Ser399, and Leu400. In the E396K mutant, the double hydrogen bond structure with Arg392 changed to a single hydrogen bond structure, and additionally, no hydrogen bond formed with Ser399 (Fig. 5D). This change could alter local stability at this site and even affect ligand binding. LigPlot+ analysis of E396K indicated ionic bond formation between Glu396 and Arg392 in the WT protein but no ionic bond formation in the mutant protein, consistent with the structural prediction (Fig. 5E). The ΔΔG predictions for the G107V and E396K mutants demonstrated that the nsSNPs could lead to poor thermal stability of PRSS56 (Table 3). Together, these computational predictions suggest that p.G107V and p.E396K may alter local structural stability of PRSS56, potentially contributing to impaired protein function.

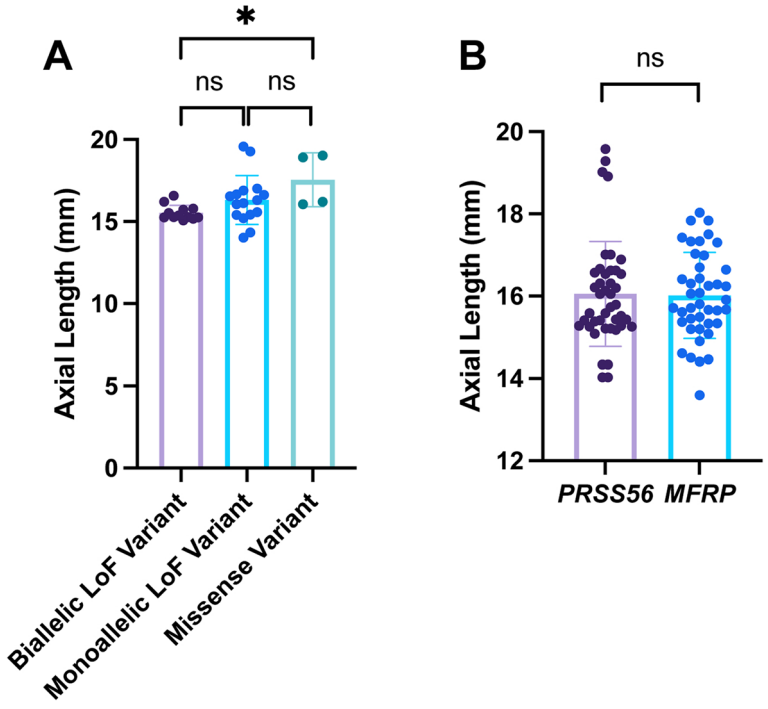

Fig. 4 Phenotype–genotype correlation in patients with *PRSS56*-associated microphthalmia. **A** Comparison of AL among eyes with different variants in the *PRSS56* gene. $n = 12$, 16, and 4, respectively. **B** Comparison of AL between eyes with *PRSS56*-associated microphthalmia and those with *MFRP*-associated microphthalmia. $n = 40$ and 42, respectively. AL: axial length. LoF: loss-of-function. * indicates $P < 0.05$, and ns indicates no statistical significance. These figures showed pooled analysis combining eyes from the current cohort and previously published cases with extractable individual-level AL data. Given the limited sample size in some subgroups, this analysis should be considered exploratory

Discussion

In this study, *PRSS56* variants were identified in four Chinese families, accounting for 57.14% of all microphthalmia families. Seven variants were identified: two novel and five previously reported. Our cohort of Chinese patients with microphthalmia harbouring *PRSS56* variants expanded the mutation spectrum of *PRSS56* in this population. However, two of the identified variants, c.175G > A:p.E59K and c.1030 C > A:p.P344T, remain VUS under current ACMG criteria. Therefore, their contribution to disease should be interpreted cautiously, particularly in the absence of complete segregation data or functional validation.

In 2011, Gal et al. [16] first identified biallelic *PRSS56* variants in autosomal recessive posterior microphthalmia. To date, approximately 70 pathogenic variants associated with the phenotypes of microphthalmia, high hyperopia, and ACG have been documented in *PRSS56* [7, 10, 16]. In previous studies, LoF variant was the most common mutation type in *PRSS56*, but in our study, missense variant was the most frequent type (71.43%). The hotspot regions of *PRSS56* in previous studies (from diverse ethnic groups including Chinese, Caucasian/European, Turkish, Kurdish, Japanese, Arab, and South Asian) are located in exons 4, 7, and 13, whereas the variants in our study are predominantly located in exon 9, and the main distribution in the Chinese population is in exons 4, 6, 7, 8 and 9. Among the five known variants, two (c.632G > C:p.C211S and c.1186G > A:p.E396K) were reported exclusively in Chinese patients with nanophthalmos or hyperopia [10, 29, 30], which might be hotspot variants in the Chinese population. Notably, p.Q356Pfs*152 is prevalent across various ethnicities, making up more than half of all *PRSS56*-associated microphthalmia families [7, 9, 17, 31], reaffirming its significance as a mutational hotspot worldwide.

Most cases with nanophthalmos and posterior microphthalmia are explained by pathogenic variants in *PRSS56* and *MFRP*, accounting for 24.53%-90.47% of previous reports from diverse ethnicities [2, 7, 9, 31]. In our previous trio-based whole-genome sequencing study of 24 Chinese probands with nanophthalmos, the detection rates of *PRSS56* and *MFRP* were 29.16% (7/24) [2]. Nonetheless, in this study, variants in *PRSS56* explained 57.14% of the probands. In the Beijing Tongren nanophthalmos with secondary angle-closure glaucoma cohort reported by Yu et al., *PRSS56* accounted for 20 of 88 patients overall (20/88, 22.7%) [32]. In a Chinese nanophthalmos cohort reported by Tao et al., the genetic diagnostic rate of *PRSS56* was 44.18% (19 *PRSS56*-related patients in 43 unrelated pedigrees) [27]. In a large Chinese nanophthalmos cohort (105 unrelated cases) reported by Xu et

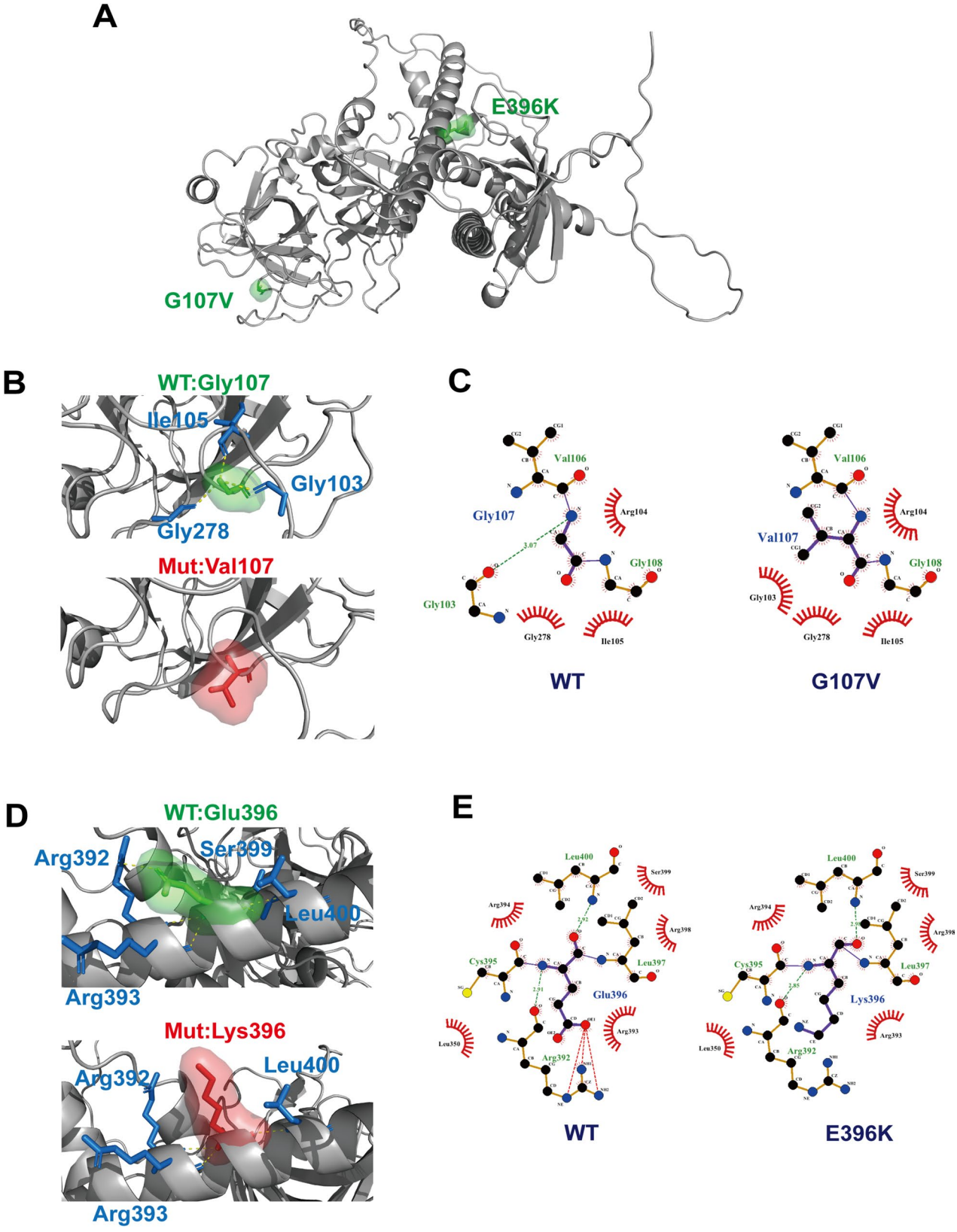

Fig. 5 (See legend on next page.)

(See figure on previous page.)

Fig. 5 Protein structure prediction of wild-type (WT) and mutant PRSS56. **A** Structure of the PRSS56 protein. Green areas indicate the location of p.G107V and p.E396K variants, respectively. **B** Conformational changes evaluated by PyMOL of G107V. WT: Gly107 forms hydrogen bonds with Gly103, Ile105, and Gly278. G107V: Val107 loses the hydrogen bonds with the surrounding amino acids. **C** LigPlot+ analysis of G107V reveals that WT protein Gly107 has hydrogen bonds with Gly103, but not with Ile105 and Gly278. Mutant protein G107V presents the loss of hydrogen bonds between Val107 and Gly103. Green dashed lines represent hydrogen bonds, and radiating arcs indicate nonbonded interactions between the target amino acid and other protein residues. **D** Conformational changes evaluated by PyMOL of E396K. WT: Glu396 is located in the α-helix structure and forms hydrogen bonds with Arg392, Arg393, Ser399, and Leu400. E396K: The dihydrogen bond is altered to a monohydrogen bond between Lys396 and Arg392, and the hydrogen bond between Lys396 and Ser399 breaks. **E** LigPlot+ analysis of E396K indicates that ionic bonds form between Glu396 and Arg392 in the WT protein, while no ionic bond formation occurs in the mutant protein. Green dashed lines represent hydrogen bonds, orange dashed lines indicate ionic bonds, and radiating arcs indicate nonbonded interactions between the target amino acid and other protein residues

al. from Shanghai Eye & ENT Hospital, biallelic *PRSS56* variants were identified in 30 cases (30/105, 28.6%) [33]. The difference in prevalence among studies might be due to differences in sample size, ethnic backgrounds, and inclusion criteria.

Cases with known consanguinity and shorter ALs are more likely to be explained by variants in *PRSS56* and *MFRP* [9, 28], particularly in eyes with biallelic LoF variants in *PRSS56.* Our exploratory pooled analysis demonstrated that eyes with biallelic variants in *PRSS56* had shorter ALs than those with missense variants in *PRSS56*, whereas eyes with biallelic LoF variants did not exhibit significantly reduced ALs compared with eyes with monoallelic LoF variants. The mechanisms by which missense *PRSS56* variants contribute to disease remain unclear. At present, these variants may affect protein stability or function, but whether they act through LoF, gain-of-function, or other mechanisms remains unknown. Interestingly, while previous studies revealed that compared with eyes with *MFRP*-associated variants, eyes with *PRSS56* variants with microphthalmia presented more severe phenotypes, including a shorter AL, a greater degree of spherical equivalent, greater corneal power and a smaller cornea diameter [9, 10, 28], our findings did not reveal a significant difference in ALs between these groups within our cohort. These findings underscore the complexity of genotype–phenotype correlations and suggest the influence of additional genetic or environmental factors. However, this finding should be interpreted cautiously given the small sample size of the missense group and the heterogeneity inherent to pooled case data.

Notably, a *PRSS56* locus SNP was found contributing to the polygenic architecture of refractive error/myopia in a GWAS of refractive error [11], which appears to be inconsistent with the hyperopic microphthalmia caused by *PRSS56* pathogenic variants. One possible explanation is that common variants exert relatively modest regulatory effects, leading to subtle changes in ocular growth, whereas rare damaging variants, especially LoF variants, may result in a much greater disruption of PRSS56 function and consequently more marked axial shortening. Alternative explanations include linkage disequilibrium, tissue-specific regulation, effects from nonaxial components, or gene–environment interactions during emmetropization. However, these explanations remain hypotheses rather than established mechanisms. A similar pattern may be seen at the *MYO1D/TMEM98* locus, where common variants contribute to the refractive error/myopia [11], while rare pathogenic *TMEM98* variants cause nanophthalmos [34]. Together, these findings suggest that different classes of variants at the same gene or locus may have distinct effects on ocular growth.

PRSS56-associated microphthalmia follows autosomal recessive inheritance. For families in which biallelic *PRSS56* variants are confirmed, the recurrence risk is 25% for each pregnancy when both parents are carriers. We suggest prioritizing targeted testing for known familial variants, such as p.Q356Pfs152, and offering prenatal diagnosis or preimplantation genetic testing in high-risk families. From a clinical counseling perspective, affected individuals with *PRSS56*-associated microphthalmia should undergo regular ophthalmic follow-up, with particular attention to anterior chamber configuration, IOP, and signs of AC. The follow-up interval depends on age and ocular biometric severity. Routine cases may be examined every 6 to 12 months. Patients with shallow anterior chambers or prior angle-closure episodes require closer surveillance, including gonioscopy and UBM or AS-OCT every 6 months to monitor anterior chamber angle status. For asymptomatic relatives, routine genetic testing and ophthalmic examination may be considered in families with confirmed biallelic familial variants, especially when early biometric changes could alter monitoring or treatment decisions. While newborn screening is reasonable in high-risk families for early ophthalmic surveillance and the management of complications such as glaucoma, population-level screening is not proposed because of the rarity of this condition.

This study has several limitations. First, incomplete clinical data and unavailable parental testing in families Z2 and Z5 precluded confirmation that the two detected variants were in trans, while the VUS status of p.E59K and p.P344T further limited the strength of ACMG interpretation and the certainty of recessive inheritance in these families. Second, the lack of long-term follow-up for these patients prevented us from assessing progression or changes in refractive status and retinopathy over

Table 3 ΔΔG prediction of the G107V and E396K variants

Mut	DUET*	SDM*	mCSM*	Prediction
G107V	-0.535	-1.78	-0.43	Destabilizing
E396K	-0.413	-0.58	-0.603	Destabilizing

ΔΔG Delta Delta G, *Mut* Mutation, *DUET* Stability Change upon Mutation (a protein stability prediction server), *SDM* Site Directed Mutator, *mCSM* Mutation Cutoff Scanning Matrix

*Positive values indicate that the variant is more stable, while negative values indicate destabilizing

time. Third, structural variants, exon-level copy-number variants below the detection threshold of our pipeline, deep intronic variants, or regulatory variants outside captured regions may have contributed to disease in the three unsolved families but would not be reliably identified by the present approach. Moreover, the protein structure predictions cannot directly confirm protein function, and we lack relevant experimental validation. In future studies, it would be valuable to incorporate genetic testing for all family members to better understand inheritance patterns, increase the sample size to further describe genotype–phenotype correlations, and establish a more comprehensive follow-up protocol to track refractive changes and other clinical outcomes over extended periods. Moreover, generating cell lines and animal models with *PRSS56* variants might also be helpful for studying the functional mechanism involved.

Conclusions

In conclusion, our study identified seven *PRSS56* variants, two of which were novel, across four Chinese families with microphthalmia. The reported variant c.1066dupC; p.Q356Pfs*152 emerged as the most frequent variant in our cohort. In an exploratory pooled analysis, eyes with biallelic variants exhibited shorter ALs than those with missense variants in *PRSS56*. Uncovering additional genetic and molecular pathways involved in microphthalmia will lead to significant insights into the growth and development of the eyeball and ultimately improve clinical care and the development of targeted therapies for affected individuals.

Supplementary Information

The online version contains supplementary material available at https://doi.org/10.1186/s12920-026-02376-9.

Supplementary Material 1.

Authors' contributions

JL analysed and interpreted the patient data, drafted the manuscript, and was a major contributor to writing the manuscript. KL, RY, and MT contributed to patient enrolment, examination, data analysis and data collection. JG designed and organized the study and modified the manuscript. All the authors reviewed the manuscript.

Funding

This work was supported by grants from the National Natural Science Foundation of China (82271083), Guangdong Basic and Applied Basic Research Foundation (A1515010914), the National Key R&D Program of China (2018YFA0108304), and the State Key Laboratory of Ophthalmology (2025QZSPT46).

Data availability

The variant's data are available in the ClinVar repository with the following accession numbers: SCV006550682, SCV006550683, SCV006550684, SCV006550685, SCV006550686, SCV006550687, and SCV006550688.

Declarations

Ethics approval and consent to participate

The study was approved by the Ethics Committee of Zhongshan Ophthalmic Center, Sun Yat-sen University (2021KYPJ192) and followed the principles of the Declaration of Helsinki. Informed consent was obtained from all the participants.

Consent for publication

All the participants/patients provided written informed consent for their personal and clinical details and for the identification of the images to be published in this study.

Competing interests

The authors declare no competing interests.

Received: 1 November 2025 / Accepted: 13 April 2026
Published online: 21 April 2026

References

1. Carricondo PC, Andrade T, Prasov L, Ayres BM, Moroi SE, Nanophthalmos. A Review of the Clinical Spectrum and Genetics. J Ophthalmol. 2018;2018:2735465. https://doi.org/10.1155/2018/2735465.
2. Guo C, Zhao Z, Chen D, et al. Detection of Clinically Relevant Genetic Variants in Chinese Patients With Nanophthalmos by Trio-Based Whole-Genome Sequencing Study. Invest Ophthalmol Vis Sci Jul. 2019;1(8):2904–13. https://doi.org/10.1167/iovs.18-26275.
3. Sener EC, Mocan MC, Sarac OI, Gedik S, Sanac AS. Management of strabismus in nanophthalmic patients: a long-term follow-up report. Ophthalmology Jun. 2003;110(6):1230–6. https://doi.org/10.1016/S0161-6420(03)00267-7.
4. Huang J, Ling Y, Lin M, Wu Z, Cheng B, Ge J. Ten-year follow-up of familial nanophthalmos in three siblings. Eye Sci Sep. 2013;28(3):113–8.
5. Zhong Y, Guo X, Xiao H, et al. Flat Anterior Chamber after Trabeculectomy in Secondary Angle-Closure Glaucoma with BEST1 Gene Mutation: Case Series. PLoS ONE. 2017;12(1):e0169395. https://doi.org/10.1371/journal.pone.0169395.
6. Luo J, Lin M, Guo X, et al. Novel BEST1 mutations and special clinical characteristics of autosomal recessive bestrophinopathy in Chinese patients. Acta Ophthalmol May. 2019;97(3):247–59. https://doi.org/10.1111/aos.13994.
7. Prasov L, Guan B, Ullah E, et al. Novel TMEM98, MFRP, PRSS56 variants in a large United States high hyperopia and nanophthalmos cohort. Sci Rep Nov. 2020;17(1):19986. https://doi.org/10.1038/s41598-020-76725-8.
8. Tao J, Luo J, Li K, Yang R, Lin Y, Ge J. Comprehensive genetic analysis uncovers the mutational spectrum of MFRP and its genotype-phenotype correlation in a large cohort of Chinese microphthalmia patients. Gene Oct. 2024;30:926:148647. https://doi.org/10.1016/j.gene.2024.148647.
9. Siggs OM, Awadalla MS, Souzeau E, et al. The genetic and clinical landscape of nanophthalmos and posterior microphthalmos in an Australian cohort. Clin Genet May. 2020;97(5):764–9. https://doi.org/10.1111/cge.13722.
10. Jiang D, Yang Z, Li S, et al. Evaluation of PRSS56 in Chinese subjects with high hyperopia or primary angle-closure glaucoma. Mol Vis. 2013;19:2217–26.
11. Tedja MS, Wojciechowski R, Hysi PG, et al. Genome-wide association meta-analysis highlights light-induced signaling as a driver for refractive error. Nat Genet Jun. 2018;50(6):834–48. https://doi.org/10.1038/s41588-018-0127-7.
12. Nair KS, Hmani-Aifa M, Ali Z, et al. Alteration of the serine protease PRSS56 causes angle-closure glaucoma in mice and posterior microphthalmia in

humans and mice. Nat Genet Jun. 2011;43(6):579–84. https://doi.org/10.1038/ng.813.
13. Paylakhi S, Labelle-Dumais C, Tolman NG, et al. Muller glia-derived PRSS56 is required to sustain ocular axial growth and prevent refractive error. PLoS Genet Mar. 2018;14(3):e1007244. https://doi.org/10.1371/journal.pgen.1007244.
14. Labelle-Dumais C, Pyatla G, Paylakhi S, et al. Loss of PRSS56 function leads to ocular angle defects and increased susceptibility to high intraocular pressure. Dis Model Mech May. 2020;29(5). https://doi.org/10.1242/dmm.042853.
15. Sen P, Robson AG, Webster AR, Nicholson L, Sivaprasad S, Hykin PG. Long-term follow-up of a case of posterior microphthalmos (PRSS56) with hyperautofluorescent retinal pigment epithelial deposits. Eur J Ophthalmol Jan. 2022;32(1):NP163–7. https://doi.org/10.1177/1120672120949756.
16. Gal A, Rau I, El Matri L, et al. Autosomal-recessive posterior microphthalmos is caused by mutations in PRSS56, a gene encoding a trypsin-like serine protease. Am J Hum Genet Mar. 2011;11(3):382–90. https://doi.org/10.1016/j.ajhg.2011.02.006.
17. Li X, Xiao H, Su Y, et al. Clinical features of patients with mutations in genes for nanophthalmos. Br J Ophthalmol. May 2024;14. https://doi.org/10.1136/bjo-2023-324931.
18. Rong H, Luo Z, Tang M, et al. Establishment of a Disease Model Using Patient-Specific Induced Pluripotent Stem Cells-Derived Trabecular Meshwork Cells in a Chinese Primary Open-Angle Glaucoma Mega-Pedigree. Discov Med. Oct 2024;36(189):2013–25. https://doi.org/10.24976/Discov.Med.202436189.185.
19. Li H, Durbin R. Fast and accurate long-read alignment with Burrows-Wheeler transform. Bioinformatics Mar 1. 2010;26(5):589–95. https://doi.org/10.1093/bioinformatics/btp698.
20. Auwera Gvd, O'Connor BD. Genomics in the cloud: using Docker, GATK, and WDL in Terra. First edition. ed. O'Reilly Media; 2020:xxiv, 467 pages.
21. Richards S, Aziz N, Bale S, et al. Standards and guidelines for the interpretation of sequence variants: a joint consensus recommendation of the American College of Medical Genetics and Genomics and the Association for Molecular Pathology. Genet Med. May 2015;17(5):405–24. https://doi.org/10.1038/gim.2015.30.
22. Abramson J, Adler J, Dunger J, et al. Accurate structure prediction of biomolecular interactions with AlphaFold 3. Nature Jun. 2024;630(8016):493–500. https://doi.org/10.1038/s41586-024-07487-w.
23. Laskowski RA, Swindells MB. LigPlot+: multiple ligand-protein interaction diagrams for drug discovery. J Chem Inf Model Oct. 2011;24(10):2778–86. https://doi.org/10.1021/ci200227u.
24. Pires DE, Ascher DB, Blundell TL. Jul. DUET: a server for predicting effects of mutations on protein stability using an integrated computational approach. Nucleic Acids Res. 2014;42(Web Server issue):W314-9. https://doi.org/10.1093/nar/gku411
25. Topham CM, Srinivasan N, Blundell TL. Prediction of the stability of protein mutants based on structural environment-dependent amino acid substitution and propensity tables. Protein Eng Jan. 1997;10(1):7–21. https://doi.org/10.1093/protein/10.1.7.
26. Worth CL, Preissner R, Blundell TL. SDM–a server for predicting effects of mutations on protein stability and malfunction. Nucleic Acids Res Jul. 2011;39:W215–22. https://doi.org/10.1093/nar/gkr363. (Web Server issue).
27. Tao J, Jin ZB, Shen RJ, MFRP. PRSS56, and MYRF account for 60.5% of a Chinese cohort with nanophthalmos. Clin Exp Ophthalmol Mar. 2025;53(2):194–208. https://doi.org/10.1111/ceo.14465.
28. Nowilaty SR, Khan AO, Aldahmesh MA, Tabbara KF, Al-Amri A, Alkuraya FS. Biometric and molecular characterization of clinically diagnosed posterior microphthalmos. Am J Ophthalmol Feb. 2013;155(2):361–e3727. https://doi.org/10.1016/j.ajo.2012.08.016.
29. Wen S, Min X, Zhu Y, Zhou X. Genetic analysis assists diagnosis of clinical systemic disease in children with excessive hyperopia. BMC Pediatr May. 2022;24(1):305. https://doi.org/10.1186/s12887-021-02992-7.
30. Wu W, Xu J, Yin H, Fu C, Yao K, Chen X. Heterozygous variants c.781G > A and c.1066dup of serine protease 56 cause familial nanophthalmos by impairing serine-type endopeptidase activity. Br J Ophthalmol. Apr 2022;5. https://doi.org/10.1136/bjophthalmol-2021-320909.
31. Almoallem B, Arno G, De Zaeytijd J, et al. The majority of autosomal recessive nanophthalmos and posterior microphthalmia can be attributed to biallelic sequence and structural variants in MFRP and PRSS56. Sci Rep Jan. 2020;28(1):1289. https://doi.org/10.1038/s41598-019-57338-2.
32. Yu X, Zhao H, Gao Y, et al. Genetic Spectrum and Genotype-Phenotype Correlations in a Chinese Cohort With Nanophthalmos With Secondary Angle-Closure Glaucoma. Invest Ophthalmol Vis Sci Jun. 2025;2(6):9. https://doi.org/10.1167/iovs.66.6.9.
33. Xu Q, Zhou Y, Wang J, et al. Comprehensive genetic landscapes and clinical heterogeneity in nanophthalmos: new insights from a large Chinese cohort. J Med Genet Sep. 2025;19. https://doi.org/10.1136/jmg-2025-110905.
34. Awadalla MS, Burdon KP, Souzeau E, et al. Mutation in TMEM98 in a large white kindred with autosomal dominant nanophthalmos linked to 17p12-q12. JAMA Ophthalmol Aug. 2014;132(8):970–7. https://doi.org/10.1001/jamaophthalmol.2014.946.

Publisher's note